Zinc(II) Thione and Selone Complexes: The Effect of Metal Redox Activity on Ligand-Based Oxidation

Bradley S. Stadelman,[a] Jaime M. Murphy,[a] Amanda M. Owen,[a], Rodrigo Castro-Ramírez,[b] Haydan C. Smith,[a] Caleb M. Cohen,[a] Lynn X. Zhang,[a] Craig A. Bayse,[c] Colin D. McMillen,[a] Norah Barba-Behrens,[b] and Julia L. Brumaghim[a,*]

[a]Department of Chemistry, Clemson University, Clemson, SC 29634-0973, USA

[b]Departamento de Química Inorgánica, Facultad de Química, Universidad Nacional Autónoma de México, Ciudad Universitaria, Coyoacán, México, D.F. 04510, Mexico

[c]Department of Chemistry and Biochemistry, Old Dominion University, Norfolk, VA 23518, USA

Abstract

Thione and selone ligands preferentially oxidize to protect redox active-metals from oxidation, but the effects of thione or selone coordination to a redox-inactive metal have not been examined. Therefore, Zn(II)-containing thione and selone complexes of the formulae $Zn(L)_2Cl_2$ and $[Zn(L)_4]^{2+}$ (L = *N*,*N*-dimethylimidazole thione, dmit, and selone, dmise) have been synthesized and their properties, including electronic spectra and DFT calculations, compared with analogous Fe(II) complexes. The $Zn(dmit/dmise)_2Cl_2$ complexes were also oxidized with H_2O_2, resulting in oxidation and C=S/Se bond cleavage of the dmit and dmise ligands. Electrochemical studies show that upon redox-inactive Zn(II) coordination, dmit- and dmise-based oxidation potentials decrease relative to those of analogous redox-active Fe(II) complexes, demonstrating that the redox activity of the metal ion significantly effects the redox properties of the ligands.

Keywords: thione; selone; zinc; redox activity; ligand oxidation

1. Introduction

Biological functions of the thione- (C=S) and selone- (C=Se) containing compounds ergothioneine and selenoneine (Figure 1) are intriguing but not well established [1-6]. Ergothioneine scavenges reactive oxygen species (ROS) and inhibits DNA damage, among other potential biological roles [7-13], and selenoneine is also a potent ROS scavenger [5,14,15]. In fact, ergothioneine is proposed to be an antioxidant vitamin with a biological role similar to that of glutathione [16,17]. Structurally similar methimazole is a commonly prescribed anti-thyroid drug, and a variety of imidazole thiones, including methimazole and the dimethylated analogs dmit and dmise (Figure 1) also act as metal-binding antioxidants [18,19].

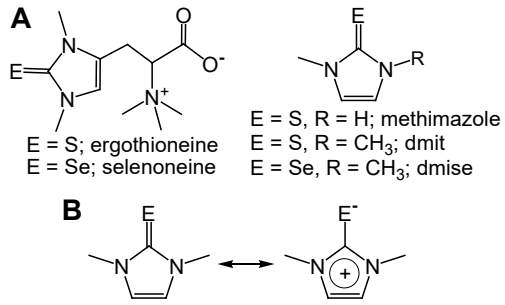

Figure 1. A) Structures of thione and selone compounds discussed in this work, and B) zwitterionic resonance structures for dmit and dmise.

Imidazole thiones and selones coordinate a variety of metal ions and coordination typically enhances the zwitterionic resonance form (Figure 1B) [20-23]. Metal coordination shifts the ligand further toward the zwitterion and enhances the electron density on the coordinated sulfur or selenium atom [22]. Metal-binding properties of imidazole thiones and selones contribute to their antioxidant activity: ergothioneine prevents *in vitro* copper-mediated oxidative DNA damage by binding copper [10], and selenoneine prevents iron oxidation by binding to Fe(II) in hemoglobin and myoglobin [6]. Zinc and iron are the most abundant *d*-block metals in the cell, followed by copper [24]. Similar to iron and copper, zinc is an essential element, fulfilling various structural,

catalytic, and regulatory roles in enzymes [25-30]. It is often coordinated to cysteine, demonstrating the stability of zinc-sulfur coordination [31], and many zinc complexes of imidazole thiones and selones are reported [32-40].

Zinc may compete with iron and copper for thione and selone binding, but unlike iron and copper, zinc is not redox active under biological conditions, and it does not generate damaging hydroxyl radicals in the presence of hydrogen peroxide [41]. Understanding the coordination and reactivity of thione and selone ligands with redox inactive metals such as zinc is essential, since dramatic differences in reactivity of coordinated sulfur ligands are observed depending on the redox activity of the coordinated metal center. In a notable example, Goldberg *et al*. [42] demonstrated that the bis(imino)pyridine-thiolate ligand (LN_3S) of the $[Fe^{II}(LN_3S)][OTf]$ complex is oxidized by O_2, but no thiolate ligand oxidation occurs upon O_2 treatment of the analogous zinc-thiolate complex. Thione or selone binding to iron or copper significantly alters ligand redox activity as well as lowering Fe(III)/(II) and Cu(II/I) electrochemical potentials [22,43]; however, the effect of zinc binding on dmit and dmise redox activity is unknown.

This work investigates the metal-specific tuning of thione and selone redox properties and oxidation that may alter their antioxidant behavior. Biologically relevant zinc complexes of thiones and selones are ideally suited for exploring the reactivity and electrochemistry of these ligands bound to a redox-inactive metal. These studies describe synthesis and characterization of the new selone complex $[Zn(dmise)_4][BF_4]_2$ (**4**) as well as development of an improved synthesis for the previously reported $[Zn(dmit)_4][BF_4]_2$ (**3**) [44]. Although the synthesis of $Zn(dmit)_2Cl_2$ (**1**) [45], and structures of $Zn(dmise)_2Cl_2$ (**2**) [34], and $[Zn(dmit)_4][BF_4]_2$ (**3**) [44] are published, we provide complete synthetic details and characterization for these complexes. In addition, we examine the reactivity of $Zn(dmit/dmise)_2Cl_2$ (**1** and **2**) with H_2O_2, and compare the electrochemistry of

analogous dmit and dmise Zn(II) and Fe(II) complexes.

2. Results and Discussion

2.1 Synthesis of Zn(II)-thione and –selone complexes

$Zn(dmit)_2Cl_2$ (**1**) was synthesized following reported procedures for $Zn(dmise)_2Cl_2$ (**2**) [34] (Scheme 1A). Synthesis of **1** and **2** were performed under atmospheric conditions, with yields of 84-86% as colorless crystals of **1** and pale-yellow crystals of **2**. Although $Zn(dmit)_2Cl_2$ (**1**) was reported previously [45], the described synthetic method (in boiling methanol) lacks detail and the complex was not fully characterized. Both complexes **1** and **2** are air stable and soluble in dimethylsulfoxide and dimethylformamide at room temperature.

To compare homoleptic complexes of dmise and dmit, $[Zn(dmise)_4][BF_4]_2$ (**4**) was synthesized according to the reaction shown in Scheme 1B. This new method was also used to synthesize the reported $[Zn(dmit)_4][BF_4]_2$ (**3**) [44] with higher yields. Treating $Zn(BF_4)_2$ with four equivalents of dmit or dmise affords colorless or yellow powders of $[Zn(dmit)_2][BF_4]_2$ (**3**) and $[Zn(dmise)_4][BF_4]$ (**4**), respectively. Syntheses of **3** and **4** were originally carried out under atmospheric conditions with ethanol as a solvent [44], but this procedure afforded less-than-

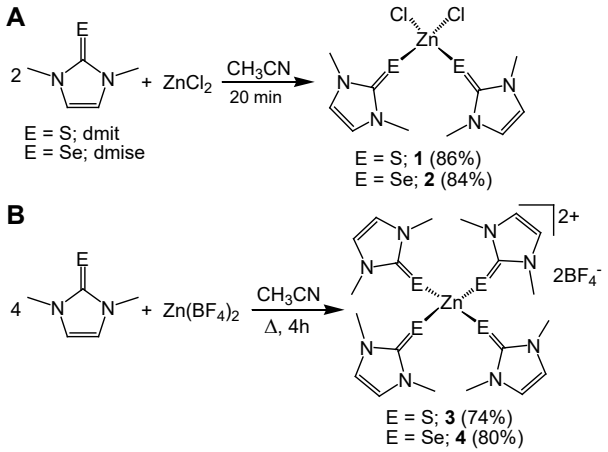

Scheme 1. Syntheses of Zn(II) thione and selone complexes **1**-**4**.

desirable yields (50-55%). Using air-free synthetic techniques increased yields of **3** and **4** to 74% and 80%, respectively. As observed for **1** and **2**, complexes **3** and **4** are air-stable in solution and in the solid state, but they are much more soluble than **1** and **2** in a variety of organic solvents.

2.2 Structural analysis of zinc-thione and –selone complexes

Structures of $Zn(dmit)_2Cl_2$ (**1**) and $[Zn(dmise)_4][BF_4]_2$ (**4**) were determined by X-ray diffraction (Figure 2 and Table 1; crystal packing diagrams are provided in Figures S1 and S2, respectively); structures of $Zn(dmise)_2Cl_2$ [34] (**2**) and $[Zn(dmit)_4][BF_4]_2$ [44] (**3**) are previously reported. Complexes **1** and **2** are an isomorphous pair, containing Zn(II) bound to two Cl atoms and two S/Se atoms from the imidazole chalcogenone (Figure 2A;). In **3** and **4**, Zn is coordinated to four S (**3**) or Se (**4**) atoms to form the tetrakis $[Zn(dmit/dmise)_4]^{2+}$ complexes, likewise forming to an isomorphous pair. Zn(II) complexes **1 - 4** are isostructural with their Fe(II) analogs [22].

All the Zn(II) centers adopt a distorted tetrahedral coordination geometry, with bond angles ranging from 103.65(3) to 119.04(4) degrees for **1**, and 103.85(2) to 122.42(6) degrees for **4**. These

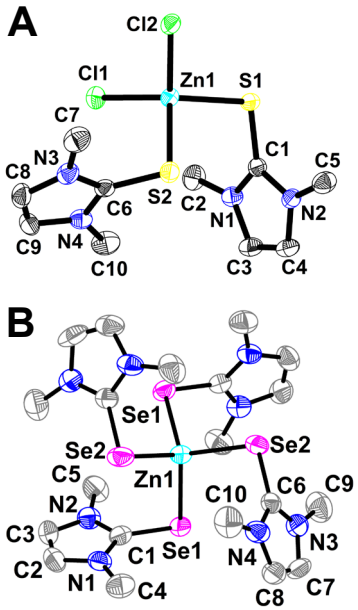

Figure 2. Crystal structure diagrams with 50% probability density ellipsoids for A) $Zn(dmit)_2Cl_2$ (**1**) and B) $[Zn(dmise)_4][BF_4]_2$ (**4**). Hydrogen atoms and counterions are omitted for clarity.

Table 1. Selected bond lengths (Å) and angles (°) for $Zn(dmit)_2Cl_2$ (**1**) and $[Zn(dmise)_4][BF_4]_2$ (**4**).

1		**4**	
Zn1—S1	2.3540 (9)	Zn1—Se1	2.4635 (9)
Zn1—S2	2.3766 (10)	Zn1—Se1^{i}	2.4635 (9)
Zn1—Cl1	2.2616 (10)	Zn1—Se2	2.4526 (10)
Zn1—Cl2	2.2865 (9)	Zn1—Se2^{i}	2.4526 (10)
S1—C1	1.713 (3)	Se1—C1	1.860 (7)
S2—C6	1.719 (4)	Se2—C6	1.850 (7)
Cl1—Zn1—S1	119.04 (4)	Se2^{i}—Zn1—Se2	122.42 (6)
Cl2—Zn1—S1	107.26 (3)	Se2^{i}—Zn1—Se1^{i}	103.85 (2)
Cl1—Zn1—S2	108.01 (4)	Se2—Zn1—Se1^{i}	104.93 (3)
Cl2—Zn1—S2	110.40 (4)	Se2^{i}—Zn1—Se1	104.93 (3)
S1—Zn1—S2	103.65 (3)	Se2—Zn1—Se1	103.85 (2)
Cl1—Zn1—Cl2	108.30 (4)	Se1^{i}—Zn1—Se1	117.88 (6)
C1—S1—Zn1	102.02 (11)	C1—Se1—Zn1	96.43 (19)
C6—S2—Zn1	100.55 (12)	C6—Se2—Zn1	96.88 (19)

i symmetry operator for symmetrically equivalent atoms: -x, y, -z+3/2.

correspond to τ_4 distortion index values [46] of 0.926 and 0.881, respectively (Table 2). Thus, the tetrakis-dmit complex appears to be more distorted about the Zn(II) center compared to the bis-dmit complex, perhaps due to the larger size of the dmise ligand in **4** compared to chloride ligand in **1**. In particular, the τ_4 index of **4** indicates a trigonal pyramidal distortion of the four-coordinate geometry. Comparable $M(dmise)_2Cl_2$ (M = Fe(II), Zn(II), Co(II)) complexes also have similar geometries (τ_4 = 0.919 to 0.981; Table 2) [22,34,47], and the τ_4 index for $Fe(dmit)_2Cl_2$ is very similar to that of **1**.

The Zn-S/Se bond lengths of the dichloride complexes **1** and **2** increase by an average of 0.02 Å compared to their tetrakis-thione and -selone analogs **3** and **4** (Table 2). This increase in

Table 2. Selected structural parameters for $M(dmit/dmise)_2Cl_2$ and $[M(dmit/dmise)_4]^{2+}$ complexes.

Complex	**τ_4**	**Average M-S/Se (Å)**	**DFT M-S/Se (Å)**	**DFT C-S/Se (Å)**	**DFT ∠ M-C-S/Se (°)**	**Reference**
$Zn(dmit)_2Cl_2$ (**1**)	0.926	2.365(1)	2.424	1.721	94.4	This work
$Fe(dmit)_2Cl_2$	0.929	2.382(1)	2.437	1.721	97.0	[22]
$[Zn(dmit)_4]^{2+}$ (**3**)	0.872	2.346 (1)	2.384	1.733	106.0	[44]
$[Fe(dmit)_4]^{2+}$	0.881	2.345(1)	2.381	1.735	108.2	[22]
$Zn(dmise)_2Cl_2$ (**2**)	0.930	2.478(1)	2.543	1.877	90.2	[34]
$Fe(dmise)_2Cl_2$	0.919	2.501(1)	2.555	1.875	92.8	[22]
$Co(dmise)_2Cl_2$	0.981	2.346(1)				[47]
$[Zn(dmise)_4]^{2+}$ (**4**)	0.881	2.457(1)	2.511	1.889	104.0	This work
$[Fe(dmise)_4]^{2+}$	0.846	2.455(1)	2.501	1.888	106.7	[22]

bond length can be attributed to a stronger electrostatic contribution to the bonding in the cationic**3** and **4**, a trend similarly observed for their iron analogs [22].

The average Zn-S bond length of $Zn(dmit)_2Cl_2$ (**1**; 2.365(1) Å) is shorter than the Fe-S bond length of $Fe(dmit)_2Cl_2$ (2.382(1) Å [22]) by 0.017(1) Å, and the average Zn-Se bond length of 2.478(1) Å is shorter than that of its iron analog, $Fe(dmise)_2Cl_2$ (2.501(1) Å [22]), by 0.023(1) Å. The shorter M-S/Se bond lengths for zinc complexes **1** and **2** compared to their Fe(II) analogs is expected due the smaller ionic radius of Zn(II) compared to high-spin Fe(II).

The Zn-S bond length in $[Zn(dmit)_4]^{2+}$ (**3**; 2.346(1) Å) is not significantly different than the Fe-S bond length of its iron analog $[Fe(dmit)_4]^{2+}$ (2.345(1) Å [22]). The same is true for the Zn-Se and Fe-Se bond lengths of their selenium analogs $[Zn(dmise)_4]^{2+}$ (**4**; 2.457(1) Å) and $[Fe(dmise)_4]^{2+}$ (2.455(1) Å [22]). The M-S/Se bond length difference seen for **1** and **2** compared to their iron analogs (and expected due to their differences in ionic radii) is not observed for the Zn-S/Se bond lengths in **3** and **4**, indicating weaker Zn-S/Se bonds compared to Fe-S/Se bonds, and potentially stronger C=S/Se bonds in these homoleptic Zn complexes.

Average C-S bond distances in **1** (1.716(4) Å) are comparable to those of other $M(L)_2Cl_2$ (M = Fe(II), Cu(II), Zn(II), Ni(II), Pd(II), Au(II), Hg(II) and L = thione) complexes, ranging from 1.705(2) to 1.722(1) Å [22,48-56]. For **4**, the observed Zn-Se bond distances average 2.46(1) Å, comparable to Fe-Se distances in $[Fe(dmise)_4]^{2+}$ (2.454(1) Å [22]). The average C-Se bond distance of 1.855(7) Å in **4** is similar to other first row transition metal-selone complexes (1.862(3) – 1.873(6) Å) [22,34,47].

2.3 DFT calculations

The DFT-optimized geometries of **1** – **4** are consistent with experimental structures, except

that the ligands in **1** and **2** adopt a C_2 orientation with short intramolecular $CH_{Im}\cdots Cl$ contacts, similar to the C_{2v} gas-phase geometries of the Fe(II) analogs [22], rather than the skewed ligand arrangement shown in Figure 2A. These differences can be attributed to the lack of intermolecular π-stacking and $CH_{Im}\cdots Cl$ interactions that determine packing in the X-ray structure. The more symmetric gas-phase DFT structure may be more representative of the solution-phase orientation of these molecules. The orientations of the zwitterionic dmit/dmise ligands are consistent with other π-donating ligands like thiolates/selenolates that coordinate with near 90° M-C-S/Se angles in both the Zn(II) and Fe(II) complexes (Table 2). Steric interactions in the tetrakis complexes lead to a roughly 10° increase in this angle. Wiberg bond indices [57] (WBI; Table S1) for the Zn-S/Se bonds are consistent with increased zwitterionic character (Figure 1B) [21,22] upon coordination as reflected in the shift toward longer C-S/Se bonds with single bond character in the complexes (i.e., $WBI_{C\text{-}S}$ = 1.429 (dmit), 1.165 (**3**); $WBI_{C\text{-}Se}$ = 1.334 (dmise), 1.086 (**4**)). The shorter Zn–S bond distances in **1** and **2** relative to their iron analogs could be attributed to either the smaller covalent radius of the Zn(II) center or a reduction in repulsions between the S/Se lone pairs and the filled, Zn(II) *d* orbitals. The greater similarity in structure and bond distance between **3** and **4** and their Fe(II) analogs may be due to greater contribution from steric interactions between the dmit/dmise ligands.

2.4 Electronic spectra

Unbound dmit and dmise ligands in the solid state show a single π→π* excitation due to imidazole ring conjugation [58] at 32,980 and 31,490 cm^{-1}, respectively (Figure S3), where the energy difference is due to the imidazole substitution by sulfur or selenium. Electronic spectra for $Zn(dmit)_2Cl_2$ (**1**), $Zn(dmise)_2Cl_2$ (**2**), and $[Zn(dmise)_4][BF_4]_2$ (**4**) show a similar band in the 25,000-

30,000 cm^{-1} region (Figures S4-S5A). In the electronic spectrum of $[Zn(dmit)_4][BF_4]_2$ (**3**; Figure S5B), this charge-transfer band is not observed. The analogous tetrahedral Fe(II) complexes also show similar electronic transition bands in the region of 29,800-32,120 cm^{-1}. Additionally, the analogous Fe(II) compounds present the expected $^5E \leftarrow {}^5T_2$ transition for a d^6 tetrahedral coordination compound (discussed in detail in Supplementary Material section and Figures S6-S9).

2.5 Infrared spectroscopy

Upon complexation with Zn(II), the bis-thione complex $Zn(dmit)_2Cl_2$ (**1**) shows a C=S stretching vibration at 1172 cm^{-1} (DFT: 1210 cm^{-1}), slightly shifted to lower energy compared to unbound dmit (1181 cm^{-1} [23]; DFT: 1215 cm^{-1} [22]). In contrast to **1**, $Zn(dmise)_2Cl_2$ (**2**) has a C=Se stretching vibration at 1149 cm^{-1} (DFT: 1182 cm^{-1}), not significantly different from unbound dmise (1148 cm^{-1} [32]; DFT: 1177 cm^{-1} [22]). The tetrakis-thione complex **3** also shows no significant shift of the C=S stretching vibration (1180 cm^{-1}; DFT: 1201 cm^{-1}) compared to unbound dmit, and the tetrakis-selone complex **4** has a C=Se stretching vibration (1146 cm^{-1}; DFT: 1179 cm^{-1}) similar to that of unbound dmise. Similar changes in S/Se=C stretching energies upon metal binding are also observed for $[Tpm^RCu(dmit)]^+$ [59], $Fe(dmit)_2Cl_2$, and $[Fe(dmit)_4]^{2+}$ [22,43]. These IR results suggest that the Zn-bound dmit/dmise C=S/Se character changes only slightly, if at all, when bound to Zn as previously observed for their Fe(II) analogs [22].

2.6 NMR spectroscopy

Due to the limited solubility of **1** and **2**, ^1H NMR spectra of complexes **1**-**4** as well as unbound dmit and dmise ligands were acquired in deuterated dimethylsulfoxide. For $Zn(dmit)_2Cl_2$

(**1**), the methyl and imidazole proton resonances shift slightly downfield (δ 3.54 and 7.32, respectively) compared to unbound dmit (δ 3.43 and 7.10, respectively). However, in $[Zn(dmit)_4][BF_4]_2$ (**3**), dmit resonances show no significant shifts for either the methyl or imidazole protons (δ 3.43 and 7.09, respectively) compared to unbound dmit.

Similar trends are observed in the ^{1}H NMR spectra of the Zn-dmise complexes. A slight downfield shift is observed for both the methyl and imidazole proton resonances of $Zn(dmise)_2Cl_2$ (**2**) (δ 3.56 and 7.38, respectively) compared to unbound dmise (δ 3.52 and 7.30, respectively). The ^{1}H NMR spectrum of $[Zn(dmise)_4][BF_4]_2$ (**4**) shows no resonance shifts for the dmise methyl and imidazole protons (δ 3.52 and 7.30, respectively). Gas-phase MALDI-TOF mass spectrometry results are consistent with Zn^{2+} coordination of the dmit/dmise ligands in complexes **1**-**4**, with observation of molecular ion as well as fragmented species for all four complexes.

Downfield shifts observed for the ^{1}H NMR resonances of bis-thione and -selone complexes **1** and **2** indicate that when two dmit ligands are bound to Zn(II), the chalcogenone ligands show more aromatic character than unbound dmit and dmise, possibly due to a shift toward a zwitterionic resonance structure [22]. In contrast, the ^{1}H NMR data for the tetrakis-thione and –selone complexes **3** and **4** indicate no significant resonance structure shift (δ 7.10 and 7.32, respectively) compared to unbound dmit and dmise, consistent with structural and IR data and suggesting weaker Zn-ligand binding in the tetrakis-dmit/dmise complexes compared to the bis-dmit/dmise complexes.

The ^{13}C[50] NMR resonances for the C=S carbon atoms in **1** and **3** are at δ 161.6 and 161.9, respectively, shifted slightly upfield from unbound dmise (δ 162.4) but significantly less shifted than the C=S resonances for the $[Tp^RCu(dmit)]^+$ complexes (δ 154.7-159.5) [59]. The C=Se resonances of **2** and **4** (δ 154.8 and 155.1, respectively) are also shifted slightly upfield compared

to unbound dmise (δ 155.6), but these relative shifts are again much smaller than those for the $[Tp^RCu(dmise)]^+$ complexes (δ 147.6-153.2). NMR comparisons for analogous Fe(II) complexes are not possible due to paramagnetic effects in their spectra.

2.7 Oxidation studies with hydrogen peroxide

Thione and selone ligands have been studied for their ability to scavenge hydrogen peroxide and peroxynitrite [22,43,60]. Oxidation studies of unbound dmit demonstrated that 3 equivalents of H_2O_2 are required to fully oxidize unbound dmit to the *N,N'*-dimethylimidazolium cation and sulfur oxyanionic ($[SO_3H]^-$ and $[SO_4H]^-$) species [43]. Similarly, treating unbound dmise with H_2O_2 yielded similar *N,N'*-dimethylimidazolium and $[SeO_2H]^-$ products; however, only 2 equivalents of H_2O_2 are required for complete dmise oxidation [43]. Thus, unbound dmise more readily oxidizes compared to dmit. Similar dmit/dmise oxidations occur when bound to Cu(I) – without Cu(I) oxidation – when $[Tpm^*Cu(dmit/dmise)]^+$ complexes are treated with H_2O_2 [43].

^{1}H NMR titrations of $Zn(dmit)_2Cl_2$ (**1**) and $Zn(dmise)_2Cl_2$ (**2**) with H_2O_2 were performed to determine how binding a redox-inactive metal ion affects thione and selone oxidation and to compare ligand oxidation products for these Zn(II) with the previously studied Cu(I) complexes. $Zn(dmit/dmise)_2Cl_2$ solutions in deuterated dimethylsulfoxide were treated with up to six equivalents of H_2O_2 (to assure maximum complex oxidation) for 10 min prior to analysis. Upon H_2O_2 oxidation of **1**, new resonances emerge at δ 3.83, 7.67, and 9.01, corresponding to formation of the imidazolium cation (Figure 3A). This assignment is supported by IR analysis of the reaction products with an observed strong, broad O-H vibration (3410 cm^{-1}) and a S-O vibration (645 cm^{-1}) as well as by ESI-MS results ($[SO_3H]^-$; *m/z* 79.5). The ^{1}H NMR spectra of **1** treated with up to six equivalents of H_2O_2 show no change compared to the spectrum observed for treatment of **1** with

four equivalents of H_2O_2, indicating that a maximum complex oxidation of only 53% is achieved upon addition of four equivalents of H_2O_2. The reason for this incomplete oxidation is unclear, but no changes in oxidation percentages or products are observed after 24 h.

Upon treatment of $Zn(dmit)_2Cl_2$ (**1**) with one equivalent of H_2O_2, mass spectrometry of the

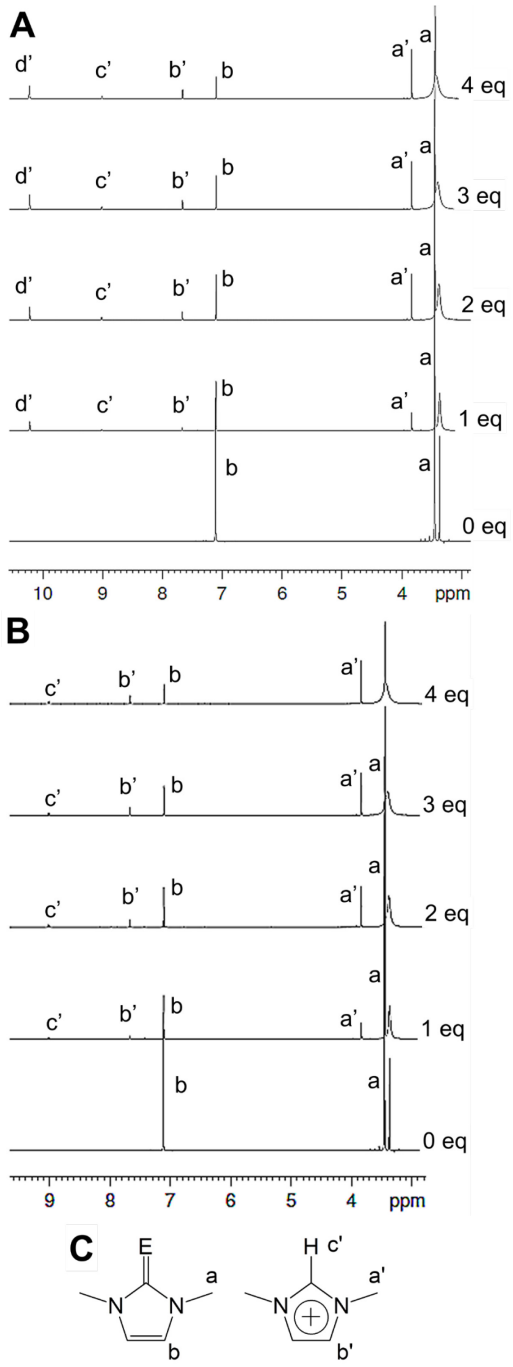

Figure 3. ^1H NMR spectra in DMSO-d_6 for A) $Zn(dmit)_2Cl_2$, B) $Zn(dmise)_2Cl_2$ upon H_2O_2 (30% in H_2O) treatment,

and C) the resonance labeling scheme, with the prime symbol indicating resonances arising from oxidation products. The resonance labeled d' could not be unambiguously unassigned.

oxidized reaction products indicate formation of *N*,*N'*-dimethylimidazolium (*m/z* 97.1), and $[SO_4H]^-$ (*m/z* 97.1) ions also are observed. In addition, very low-intensity peaks for $[dmit(OH)]^+$ corroborating ^{1}H NMR results. The Zn(II) species $[ZnCl_3]^-$ (*m/z* 169.7) is observed as the only zinc-containing product by mass spectrometry. The oxidized sulfur species $[SO_2H]^-$ (*m/z* 64.2), (*m/z* 146.6) and $[dmit(O)(OH)_2]^-$ (*m/z* 179.9) are observed, but resonances for these species are not detected in the NMR spectra, indicating that these products may be too dilute to observe or that they may be forming under mass spectrometry conditions. Treatment of unbound dmit with two or three equivalents of H_2O_2 also results in cleavage of the C=S bond to form *N*,*N'*-dimethylimidazolium and $[SO_3H]^-$ and $[SO_4H]^-$, but no oxidized dmit products are observed [43].

^{1}H NMR spectra of $Zn(dmise)_2Cl_2$ (**2**) upon 1 equiv H_2O_2 addition show a similar emergence of new resonances at δ 3.84, 7.67, and 9.07 (Figure 3B), corresponding to formation of the imidazolium cation. Upon treatment of **2** with four equivalents of H_2O_2, 85% of zinc-bound dmise becomes oxidized to the imidazolium cation, as determined by integration of the imidazole-derived proton resonances. This percentage does not increase upon adding up to six equivalents of H_2O_2 or after 24 h. Mass spectrometry data for the oxidized products again indicate formation of *N*,*N'*-dimethylimidazolium (*m/z* 97.1) as well as the oxidized selenium species $[SeO_2H]^-$ (*m/z* 113.0). Again, the sole zinc-containing species observed is $[ZnCl_3]^-$ (*m/z* 169.7). In contrast to oxidation studies of **1**, no evidence for dmise-OH species formed upon oxidation of **2** is observed by NMR spectroscopy or mass spectrometry.

Oxidation studies of $[Tpm^{Me}Cu(dmit)]^+$ [43] demonstrated that three equivalents of H_2O_2 are required to fully oxidize one equivalent of metal-bound dmit to the dimethylimidazolium cation, similar to oxidation studies with unbound dmit. In contrast, when dmit is bound to non-redox active Zn(II) in **1** and treated with up to six equivalents of H_2O_2, the two zinc-bound dmit

ligands are not completely oxidized, indicating that coordination of a redox-active metal may promote more complete H_2O_2 oxidation of metal-bound dmit and suggesting the need for electrochemical investigation of these zinc complexes.

Upon treating $[Tpm^{Me}Cu(dmise)]^+$ [43] with H_2O_2, metal-bound dmise undergoes sacrificial oxidation, protecting Cu(I) from oxidation and requiring two equivalents of H_2O_2 per dmise ligand for maximum formation (85%) of the oxidized imidazolium cation and $[SeO_2H]^-$ species, indicating that dmise undergoes sacrificial oxidation to the same degree when coordinated to both redox-active Cu(I) and non-redox active Zn(II). This result contrasts with the differential thiolate oxidation observed for $[Fe^{II}(LN_3S)][OTf]$ and $[Zn^{II}(LN_3S)][OTf]$ upon O_2 oxidation [42], suggesting that differential oxidation effects observed for redox-active and non-redox-active metal complexes may be more dependent on the S/Se ligand and/or the oxidizing species than metal redox activity.

2.6 Electrochemistry

Cyclic voltammetry was used to determine the redox potentials of complexes **1 – 4** show changes in the ligand-based waves relative to unbound dmit and dmise. Cyclic voltammograms for unbound dmit and dmise show irreversible reduction (Ep_a) and oxidation (Ep_c) waves (0.47 and -0.15 V for dmit and 0.40 and -0.12 V for dmise, respectively; Table 3 and Figure 4). Since reduction is dependent on prior oxidation these are irreversible redox reactions, and the currents measured are not from the same species. Preventing dmit or dmise reduction by starting the negative scan at 0.30 V for dmit and 0.20 for dmise results in only an oxidation wave, so an $E_{1/2}$ value for this oxidation/reduction is not meaningful [22].

Zn-dichloride complexes **1** and **2** are insoluble in acetonitrile, so cyclic voltammetry was

Table 3. Redox potentials for dmit and dmise and their Zn(II) and Fe(II) complexes vs. NHE.

	Ligand-based Potentials (V)		
Ligand or Complex	***E*pc**[a]	***E*pa**	**Reference**
dmit (DMF)	-0.15	0.47	This work
dmit (CH_3CN)	-0.14	0.59	[22]
$Zn(dmit)_2Cl_2$ (**1**) (DMF)	-0.09	0.50	This work
$[Zn(dmit)_4][BF_4]_2$ (**3**) (DMF)	-0.16	0.45	This work
$[Zn(dmit)_4][BF_4]_2$ (**3**) (CH_3CN)	-0.12	0.46	This work
$Fe(dmit)_2Cl_2$ (CH_3CN)	0.15	0.69	[22]
$[Fe(dmit)_4][OTf]_2$ (CH_3CN)	0.12	0.69	[22]
dmise (DMF)	-0.12	0.40	This work
dmise (CH_3CN)	-0.15	0.37	[22]
$Zn(dmise)_2Cl_2$ (**2**) (DMF)	-0.15	0.33	This work
$[Zn(dmise)_4][BF_4]_2$ (**4**) (DMF)	-0.15	0.19	This work
$Fe(dmise)_2Cl_2$ (CH_3CN)	0.14	0.41	[22]
$[Fe(dmise)_4][OTf]_2$ (CH_3CN)	0.11	0.36	[22]

[a]Ligand-based reduction potentials are dependent on prior oxidation, so no $E_{1/2}$ value is calculated.

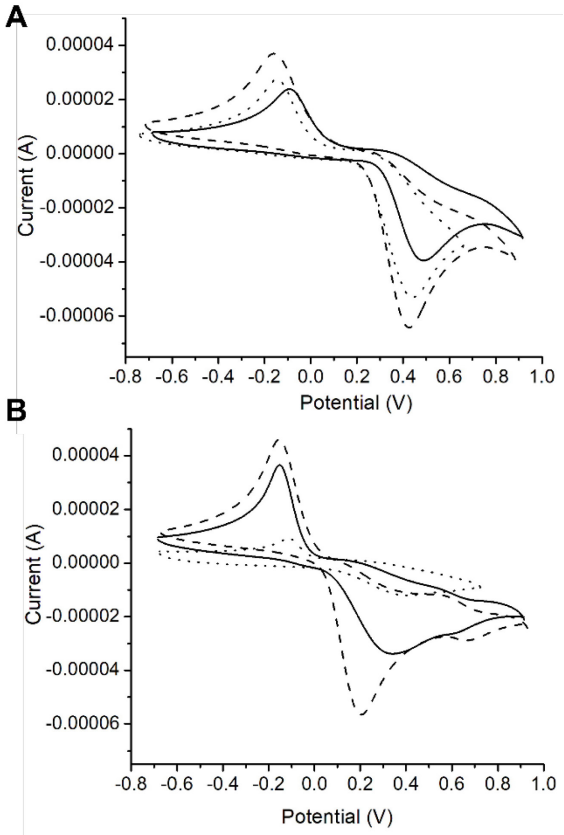

Figure 4. Cyclic voltammograms (in DMF) vs. NHE of A) $Zn(dmit)_2Cl_2$ (**1**; solid line, 10 mM), $Zn(dmise)_2Cl_2$ (**2**; dashed line, 10 mM), and dmit (dotted line, 10 mM) and B) $[Zn(dmit)_4][BF_4]_2$ (**3**; solid line, 1 mM), $[Zn(dmise)_4][BF_4]_2$ (**4**; dashed line, 1 mM), and dmise (dotted line, 1 mM). Scans were collected by sweeping the voltage from the highest potential to the lowest and back.

performed in DMF (Figure 4). To determine solvent effects and to allow direct comparisons with previous electrochemical studies of Fe-thione and selone complexes, CV for $[Zn(dmit)_4][BF_4]_2$ (**3**), dmit, and dmise were determined in both acetonitrile and DMF. In both solvents, reduction and oxidation potentials of unbound dmit and dmise were within 0.03 V, except for the oxidation potential of dmit, which becomes more positive by 0.12 V in acetonitrile compared to DMF (Table 3). Oxidation and reduction potentials of complex **3** become more positive by 0.04 and 0.01 V in acetonitrile compared to DMF (Figure 4), respectively, demonstrating only a small effect of the slightly more polar DMF on ligand potentials.

Zn(II)-dmit binding in complex **1** increases the dmit-based oxidation and reduction potentials by 0.03 and 0.06 V, respectively, indicating that the zinc-bound dmit ligand is slightly more oxidizable and reducible compared to unbound dmit. The homoleptic zinc-dmit complex **3** exhibits no significant perturbations in redox potentials compared to dmit. Electrochemical measurements at variable scan rates for $Zn(dmit)_2Cl_2$ and $Zn(dmise)_2Cl_2$ show a linear dependence of current with scan rate (Figure S10), indicating a surface-adsorbed process where the ligand-based waves are dependent on the coordinating metal (Table 3).

Although electrochemical studies determine the redox potentials of the complex as a whole, ligand-based waves are clearly identifiable in voltammograms of these zinc complexes, and the redox potentials of these waves often show significant changes upon metal coordination. This indicates that the electrochemistry of these complexes is primarily ligand-based in the observed electrochemical window, a finding that is corroborated by the calculated HOMO orbitals for these complexes as well as results of NMR studies showing preferential oxidation of the dmit or dmise ligand, even compared to redox-active copper [43].

Cyclic voltammograms of Zn(II)-dmise complexes **2** and **4** show that dmise-based

reduction potentials decrease by 0.03 V relative to unbound dmise (Table 3), indicating that dmise reduction is slightly less favorable when bound to zinc. Zinc-bound dmise-based oxidation potentials in **2** and **4** decrease by 0.07 and 0.21 V, respectively, compared to unbound dmise, indicating that zinc-bound dmise is less readily oxidizable than the unbound ligand. Thus, in **1** Zn-bound dmit is more available for redox compared to unbound dmit, but in **2**, **3**, and **4**, Zn-bound dmit or dmise is less redox-prone than the unbound chalcogenone.

The effect of redox-inactive zinc biding on dmit and dmise ligand-based redox is less significant than exhibited for $Fe(dmit/dmise)_2Cl_2$ and $[Fe(dmit/dmise)_4]^{2+}$ complexes, where the ligand-based oxidation potentials strongly increase compared to unbound dmit and dmise (Table 3). These results are consistent with the stabilization of the zinc complex HOMOs in the DFT-optimized structure of **1** - **4** by 0.30 to 0.35 eV relative to their Fe(II) analogs. Since dmit- and dmise-based oxidation potentials are significantly higher than the Fe(III/II)-based oxidation potentials, sacrificial oxidation of the ligands should occur prior to Fe(II) oxidation [22]. Interestingly, dmise-based redox potentials decrease when bound to Zn(II), making it less energetically favorable to oxidize Zn-bound dmise.

Electrochemical studies of Cu(I) complexes $[Tpm^RCu(dmit/dmise)]^+$ (Tpm^R = tris(3,5-di-R-pyrazolyl)methane; R = H, CH_3, and ^{i}Pr) [59] showed that dmit or dmise coordination decreases the Cu(II/I) redox potential by 0.35 to 0.85 V relative to Cu(I) in $[Tpm^RCu(NCCH_3)]^+$ with acetonitrile binding, potentially inhibiting catalytic metal-mediated hydroxyl radical generation [59]. Similar electrochemical studies of $Fe(dmit/dmise)_2Cl_2$ and $\{Fe(ebit/ebis)Cl_2\}_n$ complexes showed that dmit or dmise coordination decreases the Fe(III/II) redox potential by 0.34 to 0.56 V relative to $FeCl_2{\cdot}4H_2O$; however, the resulting Fe(III/II) redox potentials still fall within the window of catalytic metal-mediated hydroxyl radical generation [22].

Zn(II) is redox-inactive and does not generate damaging biological ROS, but zinc coordination also inhibits oxidation of coordinated dmit and dmise ligands by an average of 0.09 V for **1** and **2** and an average of 0.20 V for **3** and **4** relative to Fe(II) coordination, a significant fraction of the electrochemical window for metal-mediated hydroxyl radical formation (0.78 V) [61]. Our results demonstrate that the effects of metal coordination on thione and selone oxidation are substantial and should be considered when determining antioxidant activity in the presence of metal ions.

3. Conclusions

Zn(II)-thione and -selone complexes have been synthesized and characterized, and their reactivity with H_2O_2 and their electrochemical behavior have been investigated and compared to analogous Fe(II) complexes. Oxidation of $Zn(dmit)_2Cl_2$ and $Zn(dmise)_2Cl_2$ with H_2O_2 shows that dmit and dmise undergo sacrificial oxidation to cleave the C=S/Se bond and form *N*,*N*'-imidazolium and oxidized sulfur or selenium species. Dmit ligands are less readily oxidizable than dmise ligands, since a maximum of 53% dmit ligand oxidation occurs after treatment with four equivalents of H_2O_2, compared to a maximum of 85% dmise ligand oxidation after similar H_2O_2 treatment. Electrochemical studies indicate that dmit and dmise ligands are less readily oxidizable when bound to Zn(II) than when bound to Fe(II), a result consistent with calculated HOMO energies of these complexes. Thus, metal coordination can significantly impact antioxidant activity, and thione and selone compounds are more effective antioxidants when bound to hydroxyl-radical generating, redox-active Fe(II) than when bound to redox-inactive Zn(II).

4. Experimental Methods

4.1 General procedures

Synthesis of complexes **3** and **4** were carried out under an inert atmosphere of argon using standard air-free techniques. Acetonitrile (Acros), diethyl ether (Acros), zinc(II) chloride (Acros), and zinc(II) tetraflouroborate (Acros) were used as received. Dmit and dmise were synthesized following reported procedures [62]. All other reagents and solvents were used without further purification unless noted.

4.2 Instrumentation

^{1}H and $^{13}C\{^{1}H\}$ NMR spectra were obtained on a Bruker-AVANCE 300 MHz NMR spectrometer. ^{1}H and $^{13}C\{^{1}H\}$ NMR chemical shifts are reported in δ relative to tetramethylsilane (δ 0) and referenced to solvent. Infrared spectra were obtained using Nujol mulls on KBr salt plates with a Magna 550 IR spectrometer. Abbreviations used in the description of vibrational data are as follows: vs, very strong; s, strong; m, medium; w, weak; b, broad. Mass spectrometry experiments were performed on DMSO or DMF samples of the compounds using a Bruker Microflex MALDI-TOF mass spectrometer with *trans*-2-[3-(4-tert-butylphenyl)-2-methyl-2-propenyldiene (*m*/*z* 250.3) as the matrix. Electrospray ionization mass spectrometry (ESI-MS) was conducted using a SYNAPT G2 LC/MS/MS System from Waters via direct injection of sample (0.10 mL/min flow rate) into a Turbo Ionspray ionization source. Samples were run under positive and negative mode in H_2O/DMSO (5:1), with an ionspray voltage of 2500 V and 4500 V and in QTOF scan mode. All observed peak envelopes match theoretical calculations for their ions. Solid state UV–Vis–NIR spectra (diffuse reflectance) were collected from 35,000–5,000 cm^{-1} for zinc(II) coordination compounds and 35,000–4,000 cm^{-1} for Fe(II) complexes to observe the

transition at low energy. Spectra of the metal complexes were adjusted by subtracting the appropriate dmit/dmise ligand spectrum.

4.3 Electrochemistry

A three-compartment cell was used with an Ag/AgCl reference electrode, a Pt counter-electrode, and a glassy carbon working electrode. Freshly distilled dimethylformamide or acetonitrile was used as solvent with tetra-*n*-butyl ammonium hexafluorophosphate as the supporting electrolyte. Solutions containing 0.1 M electrolyte were deaerated for 10 minutes by vigorous nitrogen purge. The ferrocenium/ferrocene couple was measured under the same conditions to correct for junction potentials. The measured potentials were corrected with the measured ferrocenium/ferrocene couple vs. SCE (0.450 V for DMF and 0.400 V [63] for CH_3CN). Finally, the potentials were adjusted from SCE to NHE (-0.197 V [64]).

*4.4 Synthesis of $Zn(dmit)_2Cl_2$ (**1**)*

Dmit (327 mg, 2.55 mmol) was dissolved in boiling acetonitrile (25 mL) in an Erlenmeyer flask. $ZnCl_2$ (174 mg, 1.28 mmol) was added with stirring, and the mixture was heated at a slow boil for approximately 20 min until the reaction volume was reduced to approximately 5 mL. Colorless crystals formed upon cooling to room temperature, and the flask was covered and refrigerated for 12 h. The solution was then filtered, and the crystals were washed with cold acetonitrile and dried under vacuum. Single crystals of **1** suitable for X-ray diffraction analysis were grown as colorless rods from cold acetonitrile. Yield: 430 mg, 86%. ^{1}H NMR (DMSO-d_6): δ 3.45 (s, 6H, CH_3), 7.11 (s, 2H, CH). $^{13}C\{^1H\}$ NMR (DMSO-d_6): δ 34.5 (CH_3), 118.1 (CH), 161.6 (S=C). IR (cm^{-1}): 3149 (m), 3099 (m), 2920 (b), 2727 (w), 2671 (w), 1707 (w), 1606 (w), 1563

(s), 1463 (vs), 1378 (vs), 1241 (w), 1227 (m), 1172 (m), 1085 (m), 865 (w), 751 (s), 740 (s), 678 (s), 630 (w), 501 (m), 480 (w). MALDI-MS (*m/z*) = 228.0 $[Zn(dmit)Cl]^+$, 357.0 $[Zn(dmit)_2Cl]^+$, 392.9 $[Zn(dmit)_2Cl_2]H^+$. Anal. Calcd. for $C_{10}H_{16}Cl_2N_4S_2Zn$: C, 30.59; N, 14.27; H, 4.11. Found: C, 30.85; N, 14.30; H, 4.08. Melting point: 198-200 °C.

*4.5 Synthesis of $Zn(dmise)_2Cl_2$ (**2**)*

Complex **2** was prepared following a similar procedure as for **1** with $ZnCl_2$ (140 mg, 1.03 mmol) and dmise (380 mg, 2.06 mmol) in place of dmit. After filtration, pale yellow crystals were obtained. Yield: 420 mg, 84%. ^{1}H NMR (DMSO-d_6): δ 3.54 (s, 6H, CH_3), 7.31 (s, 2H, CH). $^{13}C\{^1H\}$ NMR (DMSO-d_6): δ 36.4 (CH_3), 120.3 (CH), 154.8 (S=C). IR (cm^{-1}): 3148 (w), 3095 (m), 2926 (b), 2727 (w), 1711 (w), 1609 (w), 1562 (m), 1456 (vs), 1378 (vs), 1242 (w), 1225 (m), 1149 (m), 1087 (m), 865 (w), 754 (s), 737 (s), 663 (m), 613 (w), 468 (m). MALDI-MS (*m/z)* = 276.0 $[Zn(dmise)Cl]^+$, 450.8 $[Zn(dmise)_2Cl]^+$, 486.8 $[Zn(dmise)_2Cl_2]H^+$. Anal. Calcd. for $C_{10}H_{16}Cl_2N_4Se_2Zn$: C, 24.69; N, 11.52; H, 3.32. Found: C, 24.92; N, 11.56; H, 3.21. Melting point: 208-210 °C (dec.).

*4.6 Synthesis of $[Zn(dmit)_4][BF_4]_2$ (**3**)*

Under argon, $Zn(BF_4)_2$ (226 mg, 0.67 mmol) was dissolved in acetonitrile (5 mL) and added to a solution of dmit (170 mg, 1.3 mmol) in acetonitrile (10 mL). The solution was stirred for 12 h, and the solvent volume was then reduced to 5 mL. The product was precipitated with diethyl ether and dried under vacuum, yielding an off-white powder. Crystals were grown by slow vapor diffusion of ether into acetonitrile. Yield: 370 mg, 74%. ^{1}H NMR (DMSO-d_6): δ 3.45 (s, 12H, CH_3), 7.10 (s, 4H, CH). $^{13}C\{^1H\}$ NMR (DMSO-d_6): δ 34.4 (CH_3), 118.0 (CH), 161.9 (S=C).

IR (cm^{-1}): 3168 (w), 3140 (w), 3115 (w), 2925 (vs, b), 2727 (w), 1570 (m), 1490 (w), 1459 (s), 1398 (w), 1377 (m), 1288 (w), 1180 (m), 1054 (s), 861 (w), 745 (m), 679 (m), 521 (w), 502 (w). MALDI-MS (*m/z)* = 288.1 $[Zn(dmit)_4]^{2+}$, 663.2 $[Zn(dmit)_4][BF_4]^+$. Anal. Calcd. for $C_{20}H_{32}B_2F_8N_8S_4Zn$: C, 31.95; N, 14.91; H, 4.29. Found: C, 31.98; N, 14.91; H, 4.29. Melting point: <260 °C.

*4.7 Synthesis of $[Zn(dmise)_4][BF_4]_2$ (**4**)*

Complex **4** was prepared using the same procedure as complex **3** except $Zn(BF_4)_2$ (180 mg, 0.53 mmol) was used and dmise (187 mg, 1.06 mmol) was used instead of dmit. Crystals of **4** were grown as yellow prisms from vapor diffusion of diethyl ether into an acetonitrile solution of **4**. Yield: 400 mg, 80%. ^1H NMR (DMSO-d_6): δ 3.54 (s, 12H, CH_3), 7.32 (s, 4H, CH). $^{13}C\{^1H\}$ NMR (DMSO-d_6): δ 36.3 (CH_3), 120.1 (CH), 155.1 (S=C). IR (cm^{-1}): 3165 (w), 3139 (w), 3106 (w), 2972 (s), 2853 (s), 1569 (w), 1459 (s), 1378 (m), 1260 (w), 1237 (m), 1146 (w), 1055 (s), 800 (w), 740 (m), 652 (w), 521 (w). MALDI-MS (*m/z)* = 383.0 $[Zn(dmise)_4]^{2+}$, 854.9 $[Zn(dmise)_4][BF_4]^+$ Anal. Calcd. for $C_{20}H_{32}B_2F_8N_8Se_4Zn$: C, 25.57; N, 11.93; H, 3.43. Found: C, 25.46; N, 11.71; H, 3.40. Melting point: <260 °C.

4.8 Reactivity of $Zn(dmit)_2Cl_2$ and $Zn(dmise)_2Cl_2$ with H_2O_2

$Zn(dmit)_2Cl_2$ (20 mg, 0.041 mmol) or $Zn(dmise)_2Cl_2$ (20 mg, 0.051 mmol) was dissolved in dimethylsulfoxide-d_6 (0.5 mL) and to this was added 1.0, 2.0, 3.0 or 4.0 equiv of H_2O_2 (0.041 , 0.082, 0.123, or 0.164 mmol; 1.45, 2.90, 4.35, or 5.80 μL; H_2O_2 concentration was measured using UV spectroscopy at 240 nm and a molar absorptivity of 43.6 $M^{-1}cm^{-1}$ [65]). The reaction mixtures were stirred for 10 min before NMR spectra were acquired. For $Zn(dmit)_2Cl_2$: yield of oxidized

product using 4 equiv H_2O_2: 53% by ^1H NMR spectroscopy. ^1H NMR (DMSO-d_6): δ 3.83 (s, 6H, $2CH_3$), 7.67 (s, 2H, 2CH), 9.01 (s, 1H, CH), 10.22 (s, 1H, $[SO_3H]^-$). MALDI-MS: *m*/*z* positive ionization: 97.1 $[C_5H_9N_2]^+$, 100.0 $[ZnCl]^+$; ESI-MS: negative ionization: 64.2 $[SO_2H]^-$, 79.5 $[SO_3H]^-$, 97.1 $[SO_4H]^-$, 169.7 $[ZnCl_3]^-$. For $Zn(dmise)_2Cl_2$: yield of oxidized product using 4 equivalents of H_2O_2: 85% by ^1H NMR spectroscopy. ^1H NMR (DMSO-d_6): δ 3.84 (s, 6H, $2CH_3$), 7.67 (s, 2H, 2CH), 9.07 (s, 1H, CH). MALDI-MS: *m*/*z* positive ionization: 97.1 $[C_5H_9N_2]^+$, 100.0 $[ZnCl]^+$; negative ionization: 113.0 $[SeO_2H]^-$, 169.7 $[ZnCl_3]^-$.

4.9 Density functional theory (DFT) calculations

All calculations were performed using Gaussian 09 [66] and the mPW1PW91 exchange correlation functional [67]. The zinc ion was represented by the Wachters-Hay all-electron basis set [68,69]. Carbon, oxygen, nitrogen and hydrogen basis sets were triple-ζ quality augmented with polarization and diffuse (C,N,O only) functions [70]. Sulfur and selenium were represented by the Wadt-Hay effective core potential basis sets [71] with additional diffuse and polarization functions. Frequency calculations were used to confirm optimized structures as minima on the potential energy surface. Wiberg bond indices (WBIs) [72,73] were calculated from the optimized structures using Natural Bond Orbital version 3.1. Time-dependent DFT calculations were performed from optimized structures and included the first 30 excitations.

4.10 Single crystal X-ray data collection

Single crystals of $Zn(dmit)_2Cl_2$ (**1**), crystallized as colorless rods, were grown from cooling the reaction mixture of acetonitrile solution. $[Zn(dmise)_4][BF_4]_2$ (**4**), crystallized as light yellow prisms, were grown from vapor diffusion of diethyl ether into an acetonitrile solution. Both crystals

were mounted on a glass filament with epoxy glue, and immediately placed on the diffractometer in a room-temperature nitrogen gas stream. Intensity data were collected using a Rigaku Mercury CCD detector and an AFC8S diffractometer. The space groups $P2_1/n$ and *Pbcn* were determined from the systematic absences for complexes **1** and **4** (Table 4). The structures were solved by direct methods and subsequent Fourier difference techniques, and refined anisotropically, by full-matrix least squares, on F^2 using SHELXTL [74]. The quantity minimized by the least squares program was $\Sigma w = (F_o^2 - F_c^2)^2$ where $w = \{[\sigma^2(F_o^2)]+(0.0307P)^2 + 1.57P\}$ where $P = (F_o^2)+2F_c^2)/3$. In the final cycle of least squares, independent anisotropic displacement factors were refined for the non-hydrogen atoms, and hydrogen atoms were fixed in idealized positions with C−H = 0.96 A.

Table 4. Summary of crystallographic data for complexes **1** and **4**.

	1	**4**
Chemical formula	$C_{10}H_{16}Cl_2N_4S_2Zn$	$C_{20}H_{32}B_2F_8N_8Se_4Zn$
F.W. (g/mol^{-1})	392.66	939.37
Space group	$P2_1/n$	*Pbcn*
Crystal system	Monoclinic	Orthorhombic
a, Å	9.3641(13)	11.9598(10)
b, Å	13.5905(16)	21.3730(19)
c, Å	13.202(2)	13.1632(10)
α, deg	90	90
β, deg	108.736(4)	90
γ, deg	90	90
V, Å^{-3}	1591.4(4)	3364.7(5)
Z	4	4
$D_{cal,}$ mg/m^3	1.639	1.854
indices (min)	[-11, -16, -15]	[-14, -25, -15]
indices (max)	[10, 15, 15]	[14, 25, 15]
parameters	176	309
F(000)	800	1824
μ, mm^{-1}	2.13	5.13
2θ range, deg	2.74-25.19	2.45-25.24
collected reflections	11422	25454
unique reflections	2859	3053
Final R (obs. data)[a], R_1	0.0371	0.0521
wR_2	0.0829	0.1332
final R (all data), R_1	0.0445	0.0642
wR_2	0.0895	0.1468
goodness of fit (S)	1.147	1.107
largest diff. peak	0.45	0.73
largest diff. hole	-0.40	-0.57

[a] $R_1 = \Sigma \| F_0| - |F_c\|/\Sigma|F_0|$; $wR_2 = \{\Sigma w(F_0^2 - F_c^2)^2\}^{1/2}$.

Isotropic hydrogen atom displacement parameters were set equal to 1.5 times U_{eq} of the attached carbon atom. For **1**, the largest peak in the final Fourier difference map (0.45 e·A^{-3}) was located 0.81 Å from H8 and the lowest peak (-0.40 e·A^{-3}) was located at a distance of 0.82 A from Zn1. For **4** the largest peak in the final Fourier difference map (0.73 e·A^{-3}) was located 0.04 Å from Zn1 and the lowest peak (-0.57 e·A^{-3}) was located at a distance of 0.88 Å from Zn1.

Conflicts of Interest

There are no conflicts of interest to declare.

Acknowledgements

J.L.B. thanks National Science Foundation grant CHE 1213912 with a Supplement for International Collaborations and CHE 1807709 for financial support. J.M.M. thanks Clemson University for a Doctoral Dissertation Completion Grant.

Appendix A. Supplemental Material

Electronic supplementary information (ESI) available: DFT coordinates for **1**-**4**, X-ray structural data for **1** and **4**, and electronic spectra. CCDC 1852325 (**1**) and 1852326 (**4**) data can be obtained free of charge at http://www.ccdc.cam.ac.uk/conts/retrieving.html. For ESI and crystallographic data in CIF or other electronic format see DOI: 10.1039/x0xx00000x.

References

[1] I.J. Briggs, Neurochemistry 19 (1972) 27-35.

[2] R.M. Epand, R.F. Epand, S.C. Wong, J. Clin. Chem. Clin. Biochem. 26 (1988) 623-626.

[3] J. Ey, E. Schomig, D. Taubert, J. Agric. Food. Chem. 55 (2007) 6466-6474.

[4] F. Franzoni, R. Colognato, F. Galetta, I. Laurenza, M. Barsotti, R. Di Stefano, R. Bocchetti, F. Regoli, A. Carpi, A. Balbarini, L. Migliore, G. Santoro, Biomed. Pharmacother. 60 (2006) 453-457.

[5] Y. Yamashita, M. Yamashita, J. Biol. Chem. 285 (2010) 18134-18138.

[6] Y. Yamashita, T. Yabu, M. Yamashita, J. Biol. Chem. 1 (2010) 144-150.

[7] B.D. Paul, S.H. Snyder, Cell Death Different. 17 (2010) 1134-1140.

[8] I.K. Cheah, L. Feng, R.M.Y. Tang, K.H.C. Lim, B. Halliwell, Biochem. Biophys. Res. Commun. 478 (2016) 162-167.

[9] L. Servillo, D. Castaldo, R. Casale, N. D'Onofrio, A. Giovane, D. Cautela, M.L. Balestrieri, Free Radic. Biol. Med. 79 (2015) 228-236.

[10] B.Z. Zhu, L. Mao, R.M. Fan, J.G. Zhu, Y.N. Zhang, J. Wang, B. Kalyanaraman, B. Frei, Chem. Res. Toxicol. 24 (2011) 30-34.

[11] T. Asahi, X. Wu, H. Shimoda, S. Hisaka, E. Harada, T. Kanno, Y. Nakamura, Y.K. Osawa, Biosci. Biotechnol. Biochem. 80 (2016) 313–317.

[12] M. Wang, Q. Zhao, W. Liu, Bioessays 37 (2015) 1262-1267.

[13] S.F. Graham, O.P. Chevallier, P. Kumar, O. Türkoğlu, R.O. Bahado-Singh, J. Perinatol. 37 (2017) 91-97.

[14] M. Klein, L. Ouerdane, M. Bueno, F. Pannier, Metallomics 3 (2011) 513-520.

[15] M. Yamashita, S. Imamura, T. Yabu, K. Ishihara, Y. Yamashita, Biomed. Res. Trace Elem. 24 (2013) 176-184.

[16] I.K. Cheah, B. Halliwell, Biochim. Biophys. Acta 1822 (2012) 784-793.

[17] B. Halliwell, I.K. Cheah, C.L. Drum, Biochem. Biophys. Res. Commun. 470 (2016) 245-250.

[18] R.C. Smith, J.Z. Gore, Biochim. Biophys. Acta 1034 (1990) 263-267.

[19] M.T. Zimmerman, C.A. Bayse, R.R. Ramoutar, J.L. Brumaghim, J. Inorg. Biochem. 145 (2015) 30-40.

[20] B.S. Stadelman, J.L. Brumaghim, Thione- and Selone-Containing Compounds, Their Late First Row Transition Metal Coordination Chemistry, and Their Biological Potential, in: Biochalcogen Chemistry: The Biological Chemistry of Sulfur, Selenium, and Tellurium, American Chemical Society, Washington, 2013, pp
33-70.

[21] Y. Rong, A. Al-Harbi, B. Kriegel, G. Parkin, Inorg. Chem. 52 (2013) 7172-7182.

[22] B.S. Stadelman, M.M. Kimani, C.A. Bayse, C.D. McMillen, J.L. Brumaghim, Dalton Trans. 45 (2016) 4697-4711.

[23] V.K. Landry, M. Minoura, K. Pang, D. Buccella, B.V. Kelly, G. Parkin, J. Am. Chem. Soc. 128 (2006) 12490-12497.

[24] R. McRae, B. Lai, C.J. Fahrni, Metallomics 5 (2013) 52-61.

[25] M. Laitaoja, J. Valjakka, J. Janis, Inorg. Chem. 52 (2013) 10983-10991.

[26] D.S. Auld, BioMetals 14 (2001) 271-313.

[27] B.L. Vallee, D.S. Auld, Biochemistry 29 (1990) 5647-5659.

[28] W.N. Lipscomb, N. Strater, Chem. Rev. 96 (1996) 2375-2434.

[29] W. Maret, Adv. Nutr. 4 (2013) 82-91.

[30] D.S. Auld, BioMetals 22 (2009) 141-148.

[31] H. Vahrenkamp, Dalton Trans. 42 (2007) 4751-4759.

[32] J.L.T. White, J. M.; Churchill, D. G.; Rheingold, A. L.; Rabinovich, D., J. Chem. Cryst. 33 (2003) 437-445.

[33] D.J. Williams, J.J. Concepcion, M.C. Koether, K.A. Arrowood, A.L. Cramack, T.G. Hamilton, S.M. Luck, M. Ndomo, C.R. Teel, D. VanDerveer, J. Chem. Cryst. 36 (2006) 453-457.

[34] D.J. Williams, K.M. White, D. VanDerveer, A.P. Wilkinson, Inorg. Chem. Comm. 5 (2002) 124-126.

[35] M. Fettouhi, M.I.M. Wazeer, A.A. Isab, Z. Kristallogr. New Cryst. Struct. 221 (2006) 221-222.

[36] T.S. Lobana, A.K. Sandhu, A.K. Jassal, G. Hundal, R.K. Mahajan, J.P. Jasinski, R.J. Butcher, Polyhedron 87 (2015) 17-27.

[37] F. Isaia, M.C. Aragoni, M. Arca, A. Bettoschi, C. Caltagirone, C. Castellano, F. Demartin, V. Lippolis, T. Pivetta, E. Valletta, Dalton Trans. 44 (2015) 9805-9814.

[38] R. Castro, J.A. Garcia-Vazquez, J. Romero, A. Sousa, Y.D. Chang, J. Zubieta, Inorg. Chim. Acta 237 (1995) 143-146.

[39] E.S. Raper, Coord. Chem. Rev. 61 (1985) 115-184.

[40] P.D. Akrivos, Coord. Chem. Rev. 213 (2001) 181-210.

[41] C. Angele-Martinez, C. Goodman, J. Brumaghim, Metallomics 6 (2014) 1358-1381.

[42] Y. Jiang, L.R. Widger, G.D. Kasper, M.A. Siegler, D.P. Goldberg, J. Am. Chem. Soc. 132 (2010) 12214-12215.

[43] M.M. Kimani, C.A. Bayse, B.S. Stadelman, J.L. Brumaghim, Inorg. Chem. 52 (2013) 11685-11687.

[44] D.J. Williams, K.A. Arrowood, L.M. Bloodworth, A.L. Carmack, D. Gulla, M.W. Gray, I. Massen, F. Rizvi, S.L. Rosenbaum, K.P. Gwaltney, D. VanDerveer, J. Chem. Crystallogr. 40 (2010) 1074-1077.

[45] D.J. Williams, P.H. Poor, G. Ramirez, B.L. Heyl, Inorg. Chim. Acta 147 (1988) 221-226.

[46] L. Yang, D.R. Powell, R.P. Houser, Dalton Trans. (2007) 955-964.

[47] D.J. Williams, T.A. Jones, E.D. Rice, K.J. Davis, J.A. Ritchie, W.T. Pennington, G.L. Schimek, Acta Crystallogr. C53 (1997) 837-838.

[48] U. Flörke, A. Ahmida, J. Schroder, H. Egold, G. Henkel, Acta Crystallogr. E69 (2013) m211.

[49] E. Flörke, A. Ahmida, H. Egold, G. Henkel, Acta Crystallogr. E70 (2014) m384.

[50] A. Ahmida, U. Florke, H. Egold, G. Henkel, Acta Crystallogr. E71 (2015) m147.

[51] J.R. Miecznikowski, M.A. Lynn, J.P. Jasinski, W. Lo, D.W. Bak, M. Pati, E.E. Butrick, A.E. Drozdoski, K.A. Archer, C.E. Villa, E.G. Lemons, E. Powers, M. Siu, C.D. Gomes, N.A. Bernier, K.N. Morio, Polyhedron 80 (2014) 157-165.

[52] C. Wang, W. Lu, Y. Tong, Y. Zheng, Y. Yang, RSC Adv. 4 (2014) 57009-57015.

[53] W. Jia, Y. Dai, H. Zhang, X. Lu, E. Sheng, RSC Adv. 5 (2015) 29491-29496.

[54] Z. Popovic, G. Pavlovic, D. Matkovic-Calogovic, Z. Soldin, M. Rajic, D. Vikic-Topic, D. Kovacek, Inorg. Chim. Acta 306 (2000) 142-152.

[55] A.M. Hutchings, N.E. McConnell, R.A. Faucher, D. VanDerveer, D.J. Williams, J. Chem. Cryst. 33 (2003) 619-623.

[56] T. Bertrand, C. Jolivalt, P. Briozzo, E. Caminade, N. Joly, C. Madzak, C. Mougin, Biochemistry 41 (2002) 7325-7333.

[57] K.B. Wiberg, Tetrahedron 24 (1968) 1083-1096.

[58] P.S. Kalsi, Spectroscopy of Organic Compounds, 6th ed., New Age International Publishers, New Delhi, 2004, pp 51-53.

[59] M.M. Kimani, J.L. Brumaghim, D. VanDerveer, Inorg. Chem. 49 (2010) 9200-9211.

[60] K.P. Bhabak, G. Mugesh, Chem. Eur. J. 16 (2010) 1175-1185.

[61] J.L. Pierre, M. Fontecave, BioMetals 12 (1999) 195-199.

[62] R. Gouriprasanna, D. Debasis, G. Mugesh, Inorg. Chim. Acta 360 (2007) 303-316.

[63] N.G. Connelly, W.E. Geiger, Chem. Rev. 96 (1996) 877-910.

[64] H.M. Koepp, H. Wendt, H.Z. Strehlow, Electrochemistry 64 (1960) 483-491.

[65] R.W. Noble, Q.H. Gibson, J. Biol. Chem. 9 (1970) 2409-2413.

[66] M.J. Frisch, G.W. Trucks, H.B. Schlegel, G.E. Scuseria, M.A. Robb, J.R. Cheeseman, G. Scalmani, V. Barone, B. Mennucci, G.A. Petersson, H. Nakatsuji, M. Caricato, X. Li, H.P. Hratchian, A.F. Izmaylov, J. Bloino, G. Zheng, J.L. Sonnenberg, M. Hada, M. Ehara, K. Toyota, R. Fukuda, J. Hasegawa, M. Ishida, T. Nakajima, Y. Honda, O. Kitao, H. Nakai, T. Vreven, J.A. Montgomery, Jr., J.E. Peralta, F. Ogliaro, M. Bearpark, J.J. Heyd, E. Brothers, K.N. Kudin, V.N. Staroverov, R. Kobayashi, J. Normand, K. Raghavachari, A. Rendell, J.C. Burant, S.S. Iyengar, J. Tomasi, M. Cossi, N. Rega, M.J. Millam, M. Klene, J.E. Knox, J.B. Cross, V. Bakken, C. Adamo, J. Jaramillo, R. Gomperts, R.E. Stratmann, O. Yazyev, A.J. Austin, R. Cammi, C. Pomelli, J.W. Ochterski, R.L. Martin, K. Morokuma, V.G. Zakrzewski, G.A. Voth, P. Salvador, J.J. Dannenberg, S. Dapprich, A.D. Daniels, Ö. Farkas, J.B. Foresman, J.V. Ortiz, J. Cioslowski, D.J. Fox, Gaussian 09 (Revision D.01), Gaussian Inc., Wallingford, CT, 2009.

[67] C. Adamo, V. Barone, J. Chem. Phys. 108 (1998) 664-675.

[68] A.J.H. Wachters, J. Chem. Phys. 52 (1970) 1033.

[69] P.J. Hay, J. Chem. Phys. 66 (1977) 4377-4384.

[70] T.H. Dunning, J. Chem. Phys. 55 (1971) 716-723.

[71] W.R. Wadt, P.J. Hay, J. Chem. Phys. 82 (1985) 284-298.

[72] J.P. Foster, F. Weinhold, J. Am. Chem. Soc. 102 (1980) 7211–7218.

[73] A.E. Reed, F. Weinhold, J. Chem. Phys. 78 (1983) 4066-4073.

[74] G.M. Sheldrick, SHELXTL, Structure Determination Software Programs (Version 6.1), Bruker Analytical X-Ray Systems Inc., Madison, WI, 2000.